ROYAL SOCIETY
OF CHEMISTRY

PAPER

Check for updates

Elasticity of connected semiflexible quadrilaterals

Mohammadhosein Razbin ![ID] ✶[a] and Alireza Mashaghi ![ID] ✶[b]

Using the positional–orientational propagator of a semiflexible filament in the weakly bending regime, we analytically calculate the probability densities associated with the fluctuating tip and the corners of a grafted system of connected quadrilaterals. We calculate closed analytic expressions for the probability densities within the framework of the worm-like chain model, which are valid in the weakly bending regime. The probability densities give the physical quantities related to the elasticity of the system such as the force–extension relation in the fixed extension ensemble, the Poisson's ratio and the average of the force exerted to a confining stiff planar wall by the fluctuating tip of the system. Our analysis reveals that the force–extension relations depend on the contour length of the system (material content), the bending stiffness (chemical nature), the geometrical angle and the number of the quadrilaterals, while the Poisson's ratio depends only on the geometrical angle and the number of the quadrilaterals, and is thus a purely geometric property of the system.

1 Introduction

Semiflexible filaments such as the cellular cytoskeletal elements (*e.g.*, actins, microtubules, and intermediate filaments) and the genomic DNA play critical roles in many biological functions and have been subjects of intense research during the recent decades.[1–34] These biofilaments take various topologies and are often confined within cellular boundaries that exert or transduce mechanical forces.[35] Moreover, the study of the mechanical properties of such semiflexible filaments is important in designing new bio- and nano-materials.[36] An important emerging field of research is structural DNA nanotechnology. Progress has been made in designing programmable nanoscale architectures through the self-assembly of synthetic oligonucleotides *via* base-pairing and other forms of intermolecular connectivity. Various topologies and spatial configurations have been designed and synthesized for various applications, from electronics and photonics to biology and nanomedicine.[37–44] One way to make such DNA nanostructures is *via* folding and assembly of DNA molecules into various topologies, the so-called DNA origami. Defined structures can be made of DNA filaments by the arrangement of nucleotides with a subnanometer precision.[45–55] The structural DNA nanotechnology provides us with a plethora of techniques to design and to make two dimensional and three dimensional nano-objects, which can be static or dynamic.[56–69]

The worm-like chain model is a commonly used model for describing the elasticity of semiflexible filaments. There are numerous studies in which elasticity of the semiflexible filaments were investigated within the framework of the worm-like chain model.[30,70–76] Next to theoretical developments, many progresses have been made in experimental characterization of semiflexible filaments (polymers) in recent decades. Powerful techniques like optical tweezers, atomic force microscopy and other force methods allow us to measure the elasticity of such filaments at the single molecule (filament) level.[77–85] In these experiments, the force–extension relation is typically measured by stretching or compressing the filament (polymer) by an external force applied to the filament's ends (or "tips"). The force–extension relation of a single filament in longitudinal direction gives stretching or compressing behavior of the filament while the force–extension relation in lateral direction gives the bending behavior of the filament. The force–extension relation can be obtained in two different ensembles, namely the fixed-extension ensemble, and the fixed-force ensemble.[86] In the fixed-extension ensemble, the displacement of the tips is fixed and the external force fluctuates due to the thermal fluctuation of the polymer. In the fixed-force ensemble, the external force exerted on the tips of the polymer is fixed, while the displacement of the tips undergoes thermal fluctuations.

Here, we study the elasticity of structures made by longitudinally connected quadrilaterals. The work is motivated by recent developments in structural DNA nanotechnology. The quadrilaterals consist of semiflexible filaments, which can be made by DNA fragments or other semiflexible polymers. In the Section 2.1, we describe the positional–orientational propagator of a semiflexible filament in the weakly bending regime based on existing theories. In the Section 2.2, we consider a

a Department of Energy Engineering and Physics, Amirkabir University of Technology, 14588 Tehran, Iran. E-mail: m.razbin@aut.ac.ir

b Medical Systems Biophysics and Bioengineering, Leiden Academic Centre for Drug Research, Leiden University, Einsteinweg 55, 2333 CC, Leiden, The Netherlands. E-mail: a.mashaghi.tabari@lacdr.leidenuniv.nl

grafted quadrilateral. In the presence of thermal fluctuations, using the positional–orientational propagator, we obtain the probability density associated with the fluctuations and calculate the force–extension relation of the tip of the quadrilateral in the fixed extension ensemble in two different direction, x and y. Also, we calculate the Poisson's ratio of the structure. Furthermore, we confine the structure by a stiff planar wall and calculate the average of the fluctuating force exerted to the wall. The force is caused by a reduction in the number of configurations available to the system, which is in turn caused by the presence of the wall. In the Section 2.3, we repeat the calculations for the case of two longitudinally connected quadrilaterals. In Section 2.4, we generalize our calculations to a system with an arbitrary number of quadrilaterals. In Section 2.5, we compare the elasticity of the structures with different number of quadrilaterals made of identical amounts of a given polymeric material. We end our article with a conclusion part.

2 Result

2.1 The positional–orientational propagator of a semiflexible filament

The physical properties of a semiflexible filament of the contour length, L is given by the Hamiltonian, $H = \frac{\kappa}{2}\int_0^L \left(\frac{dt(s)}{ds}\right)^2 ds$ where κ is the bending stiffness of the filament and $t(s)$ is the tangent vector of the filament in the arc length s. Here, we study the filament confined in a two dimensional space. In the weakly bending regime, the density probability of finding the end point of such filament at position, (x,y) with orientation, θ given the grafted tip at position, (x_0,y_0) with orientation, ω is as follows,[6,87,88]

$$
\begin{aligned}
G_L(x, y, \theta | x_0, y_0, \omega) = \frac{1}{N_L}\exp&\left[-\frac{3l_p}{L^3}((y-y_0)\cos(\omega)\right.\\
&\left. -(x-x_0)\sin(\omega))^2 - \frac{l_p}{L}(\theta-\omega)^2\right]\\
\times\exp&\left[\frac{3l_p}{L^2}((y-y_0)\cos(\omega)\right.\\
&\left. -(x-x_0)\sin(\omega))(\theta-\omega)\right]\\
\times\delta&[(x-x_0)\cos(\omega)+(y-y_0)\sin(\omega)-L].
\end{aligned}
$$

(1)

where N_L is the normalization factor, $l_p = \frac{2\kappa}{k_B T}$ is the two dimensional persistence length, $\delta[x]$ is the Dirac delta function, k_B is the Boltzmann constant and T is the temperature.

2.2 The grafted quadrilateral

Here, we study the elasticity of a grafted semiflexible quadrilateral. The quadrilateral is constructed by conjunction of four semiflexible filaments of length L. It has four corner labeled by 0, 11, 12, 21 according to Fig. 2. The conjunction angles are fixed since the length scales of the conjunction

points are much smaller than the persistence length of the filaments. We put the origin of the coordinates at graft point of the system. The probability density to find the end corner of the quadrilateral labeled by 12 at position (x_{12},y_{12}) and orientation θ_{12} is given by the following expression,

$$
\begin{aligned}
P_{\omega,1}(x_{12}, y_{12}, \theta_{12}) = \iiiiii &G_L(x_{11}, y_{11}, \theta_{11}|0, 0, \omega)\\
\times &G_L(x_{12}, y_{12}, \theta_{12}|x_{11}, y_{11}, \theta_{11}-2\omega)\\
\times &G_L(x_{21}, y_{21}, \theta_{21}|0, 0, -\omega)\\
\times &G_L(x_{12}, y_{12}, \theta_{12}+2\omega|x_{21}, y_{21}, \theta_{21}+2\omega)\\
\times &dx_{11}dy_{11}d\theta_{11}dx_{21}dy_{21}d\theta_{21}
\end{aligned}
$$

(2)

where $\omega > 0$ is the grafting angle indicated in Fig. 2. We calculate integrals in eqn (2) and obtain the following analytic expression,

$$
P_{\omega,1}(x, y, \theta) = \frac{1}{N_{\omega,1}}\exp(A\theta^2 + B\theta + C)
$$

(3)

where

$$
A = -\frac{7l_p}{L}
$$

(4)

and

$$
B = \frac{3l_p y}{2L^2\cos(\omega)}
$$

(5)

and

$$
C = -\frac{3l_p(x-2L\cos(\omega))^2}{L^3\sin^2(\omega)} - \frac{3l_p y^2}{4L^3\cos^2(\omega)}
$$

(6)

We integrate the y component and angle θ in the probability density given by eqn (3) and obtain an expression for the probability density of finding the x component of position of the corner of quadrilateral labeled by 12 at value x,

$$
\begin{aligned}
P_{\omega,1}^X(x) &= \iint P_{\omega,1}(x, y, \theta)dyd\theta\\
&= \frac{1}{N_X}\exp\left(-\frac{3l_p(x-2L\cos(\omega))^2}{L^3\sin^2(\omega)}\right)
\end{aligned}
$$

(7)

Similarly, we obtain the probability density of the position of the corner labeled by 12 at y coordinate,

$$
\begin{aligned}
P_{\omega,1}^Y(y) &= \iint P_{\omega,1}(x, y, \theta)dxd\theta\\
&= \frac{1}{N_Y}\exp\left(-\frac{3l_p y^2}{7L^3\cos^2(\omega)}\right)
\end{aligned}
$$

(8)

The probability density to find the x component of the position of the corner labeled by 12 at x_{12} and the y component
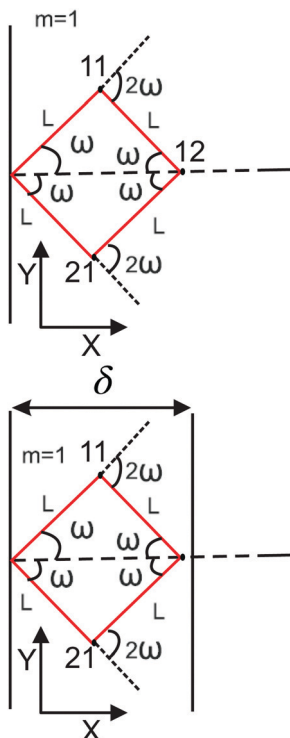
Fig. 1 The upper panel: The configuration of the grafted semiflexible quadrilateral at zero temperature. The lower panel: The grafted quadrilateral confined by a stiff planar wall.

of the position of the corner labeled by 11 at y_{11} is given by

$$
\begin{aligned}
P_{\omega,1}^{PR}(x_{12}, y_{11}) = &\iiiint\iiint G_L(x_{11}, y_{11}, \theta_{11}|0, 0, \omega) \\
&\times G_L(x_{12}, y_{12}, \theta_{12}|x_{11}, y_{11}, \theta_{11} - 2\omega) \\
&\times G_L(x_{21}, y_{21}, \theta_{21}|0, 0, -\omega) \\
&\times G_L(x_{12}, y_{12}, \theta_{12} + 2\omega|x_{21}, y_{21}, \theta_{21} + 2\omega) \\
&\times dx_{11} d\theta_{11} dx_{21} dy_{21} d\theta_{21} dy_{12} d\theta_{12}
\end{aligned}
$$

(9)

We obtain the analytic expression for the probability density after calculation of the integrals,

$$
P_{\omega,1}^{PR}(x, y_{11}) = \frac{1}{N_{PR}} \exp(A_{PR}) \tag{10}
$$

where

$$
\begin{aligned}
A_{PR} = &-\frac{24 l_p (x - 2L\cos(\omega))^2}{7} \frac{1}{L^3 \sin^2(\omega)} \\
&- \frac{12 l_p (x - 2L\cos(\omega))(y_{11} - L\sin(\omega))}{7} \frac{1}{L^3 \sin(\omega)\cos(\omega)} \\
&- \frac{12 l_p (y_{11} - L\sin(\omega))^2}{7} \frac{1}{L^3 \cos^2(\omega)}
\end{aligned}
$$

(11)

The probability densities in eqn (10), (7) and (8) give the associated force–extension relations. Using the similar method
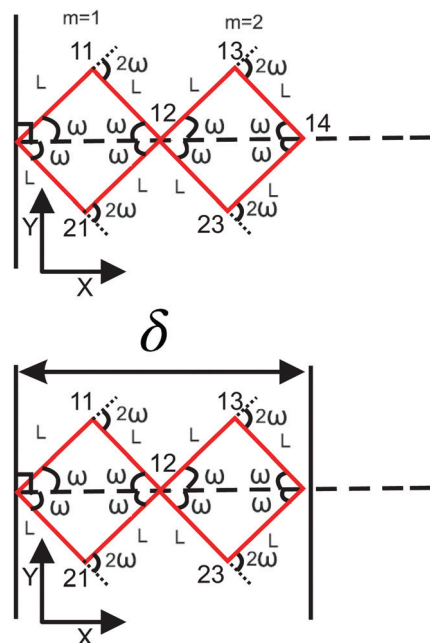

Fig. 2 The upper panel: The configuration of the grafted two longitudinally connected quadrilaterals at zero temperature. The lower panel: The two longitudinally connected quadrilaterals confined by a stiff planar wall.

in ref. 88, we obtain the analytic expression for the x coordinate of the force–extension relation associated to the corner, 12 (see Appendix),

$$
\begin{aligned}
\langle f_{\omega,1}^X(x) \rangle &= k_B T \frac{\partial}{\partial x} \ln\left(P_{\omega,1}^X(x)\right) \\
&= -\frac{6 k_B T l_p (x - H_1)}{L^3 \sin^2(\omega)}
\end{aligned}
$$

(12)

where $H_1 = 2L\cos(\omega)$ is the length of the system in the longitudinal direction at zero temperature. Similarly, the y coordinate of the force–extension relation associated to the corner, 12 is given by the following expression (see Appendix),

$$
\begin{aligned}
\langle f_{\omega,1}^Y(y) \rangle &= k_B T \frac{\partial}{\partial y} \ln\left(P_{\omega,1}^Y(y)\right) \\
&= -\frac{6 k_B T l_p y}{7 L^3 \cos^2(\omega)}
\end{aligned}
$$

(13)

The equation, $\langle f_{\omega,1}^{PR}(x, y_{11}) \rangle = \langle f_{\omega,1}^X(x) \rangle$ results in the following equation

$$
k_B T \frac{\partial}{\partial x} \ln\left(P_{\omega,1}^{PR}(x, y_{11})\right) = k_B T \frac{\partial}{\partial x} \ln\left(P_{\omega,1}^X(x)\right) \tag{14}
$$

which gives the relation between y_{11} and x (see Appendix),

$$
\frac{y_{11} - L\sin(\omega)}{x - 2L\cos(\omega)} = -\frac{1}{2}\cot(\omega) \tag{15}
$$

where $y_{11} - L\sin(\omega)$ is the displacement of the corner of the quadrilateral labeled by 11 in y coordinate due to the displacement of the corner labeled by 12 in x coordinate, $x - 2L\cos(\omega)$.

The Poisson's ratio for the grafted semiflexible quadrilateral is (see Appendix)

$$\nu_1 = -\frac{\dfrac{y_{11} - L\sin(\omega)}{w}}{\dfrac{x - 2L\cos(\omega)}{H_1}} = \frac{1}{2}\cot^2(\omega) \tag{16}$$

where $w = 2L\sin(\omega)$ is the width of the system at zero temperature. Next, we confine the system with a stiff wall in x coordinate. The confining wall reduce the number of the configuration of the system and therefore experience a fluctuating force due to the confinement. The average of the fluctuating force on the confining stiff wall is (see Appendix)

$$\left\langle f_{\omega,1}^{\text{Wall}-X}(\delta) \right\rangle = \left(\frac{12l_p}{\pi L^3}\right)^{\frac{1}{2}} \left(\frac{k_B T e^{-\frac{3l_p(\delta - H_1)^2}{L^3 \sin(\omega)}}}{A_1}\right) \tag{17}$$

where

$$A_1 = \sin(\omega)\left(\text{erf}\left(\left(\frac{12l_p}{L}\right)^{\frac{1}{2}}\cot(\omega)\right) - \text{erf}\left(\left(\frac{3l_p}{L^3}\right)^{\frac{1}{2}}\frac{H_1 - \delta}{\sin(\omega)}\right)\right) \tag{18}$$

2.3 Two longitudinally connected quadrilaterals grafted in a substrate

We connect another quadrilateral to the grafted quadrilateral according to the Fig. 2. The probability density to find the end point of the structure at position (x_{14}, y_{14}) with orientation θ_{14} is given by the following equation,

$$\begin{aligned}
P_{\omega,2}^{\text{LO}}(x_{14}, y_{14}, \theta_{14}) &= \iint \cdots \iint G_L(x_{13}, y_{13}, \theta_{13}|x, y, \theta + 2\omega) \\
&\times G_L(x_{14}, y_{14}, \theta_{14}|x_{13}, y_{13}, \theta_{13} - 2\omega) \\
&\times P_{\omega,1}(x, y, \theta)G_L(x_{23}, y_{23}, \theta_{23}|x, y, \theta) \\
&\times G_L(x_{14}, y_{14}, \theta_{14} + 2\omega|x_{23}, y_{23}, \theta_{23} + 2\omega) \\
&\times dx_{13}dy_{13}d\theta_{13}dx_{23}dy_{23}d\theta_{23}dxdyd\theta
\end{aligned} \tag{19}$$

The probability density to find the position of the end point at x coordinate in value x is

$$\begin{aligned}
P_{\omega,2}^{\text{LO},X}(x) &= \iint P_{\omega,2}^{\text{LO}}(x, y, \theta)dyd\theta \\
&= \frac{1}{N_{\omega,2}^{\text{LO},X}}\exp\left(-\frac{3}{2}\frac{l_p(4L\cos(\omega) - x)^2}{L^3(\sin(\omega))^2}\right)
\end{aligned} \tag{20}$$

Similarly, we write the probability density to find the position of the end point at y coordinate in value y according to below,

$$\begin{aligned}
P_{\omega,2}^{\text{LO},Y}(y) &= \iint P_{\omega,2}^{\text{LO}}(x, y, \theta)dxd\theta \\
&= \frac{1}{N_{\omega,2}^{\text{LO},Y}}\exp\left(-\frac{3}{38}\frac{l_p y^2}{(\cos(\omega))^2 L^3}\right)
\end{aligned} \tag{21}$$

Using the probability density, we calculate the force–extension relation in x coordinate and it takes the following form (see Appendix),

$$\begin{aligned}
\left\langle f_{\omega,2}^{\text{LO},X}(x) \right\rangle &= k_B T \frac{\partial}{\partial x}\ln\left(P_{\omega,2}^{\text{LO},X}(x)\right) \\
&= -\frac{3k_B T l_p(x - H_2)}{L^3(\sin(\omega))^2}
\end{aligned} \tag{22}$$

where the length of the system in longitudinal direction at zero temperature is $H_2 = 4L\cos(\omega)$. Also, the force–extension relation in y coordinate is (see Appendix)

$$\begin{aligned}
\left\langle f_{\omega,2}^{\text{LO},Y}(y) \right\rangle &= k_B T \frac{\partial}{\partial y}\ln\left(P_{\omega,2}^{\text{LO},Y}(y)\right) \\
&= -\frac{3k_B T}{19}\frac{l_p y}{(\cos(\omega))^2 L^3}
\end{aligned} \tag{23}$$

The probability density to find the x component of the position of the corner labeled by 14 at x_{14} and the y component of the position of the corner labeled by 13 at y_{13} is

$$\begin{aligned}
P_{\omega,2}^{\text{PR}}(x_{14}, y_{13}) &= \iint \cdots \iint G_L(x_{13}, y_{13}, \theta_{13}|x, y, \theta + 2\omega) \\
&\times G_L(x_{14}, y_{14}, \theta_{14}|x_{13}, y_{13}, \theta_{13} - 2\omega) \\
&\times P_{\omega,1}(x, y, \theta)G_L(x_{23}, y_{23}, \theta_{23}|x, y, \theta) \\
&\times G_L(x_{14}, y_{14}, \theta_{14} + 2\omega|x_{23}, y_{23}, \theta_{23} + 2\omega) \\
&\times dx_{13}d\theta_{13}dx_{23}dy_{23}d\theta_{23}dxdyd\theta dy_{14}d\theta_{14}
\end{aligned} \tag{24}$$

Similar to eqn (14) the equation in below

$$k_B T \frac{\partial}{\partial x}\ln\left(P_{\omega,2}^{\text{PR}}(x, y_{13})\right) = k_B T \frac{\partial}{\partial x}\ln\left(P_{\omega,2}^{X}(x)\right) \tag{25}$$

gives relation between the lateral and the longitudinal displacement (see Appendix),

$$\frac{y_{13} - L\sin(\omega)}{x - 4L\cos(\omega)} = -\frac{1}{4}\cot(\omega) \tag{26}$$

where $y_{13} - L\sin(\omega)$ is the displacement of the corner of the quadrilateral labeled by 13 in y coordinate due to the displacement of the corner labeled by 14 in x coordinate, $x - 4L\cos(\omega)$. Therefore, the Poisson's ratio is

$$\nu_2 = -\frac{\dfrac{y_{13} - L\sin(\omega)}{w}}{\dfrac{x - 4L\cos(\omega)}{H_2}} = \frac{1}{2}\cot^2(\omega) \tag{27}$$

Similar to the previous section, we confine the system by a stiff wall in x coordinate. The expression for the average of the

fluctuating force on the confining stiff wall due to the confinement has the following form (see Appendix),

$$
\left\langle f_{\omega,2}^{\mathrm{Wall}-X}(\delta) \right\rangle = \left(\frac{6l_{\mathrm{p}}}{\pi L^3} \right)^{\frac{1}{2}} \left(\frac{k_{\mathrm{B}} T e^{-\frac{3l_{\mathrm{p}}(\delta - H_2)^2}{2L^3 \sin(\omega)}}}{A_2} \right) \tag{28}
$$

where

$$
A_2 = \sin(\omega) \left(\mathrm{erf}\left(\left(\frac{24l_{\mathrm{p}}}{L} \right)^{\frac{1}{2}} \cot(\omega) \right) - \mathrm{erf}\left(\left(\frac{3l_{\mathrm{p}}}{2L^3} \right)^{\frac{1}{2}} \frac{H_2 - \delta}{\sin(\omega)} \right) \right) \tag{29}
$$

2.4 N number of the longitudinally connected quadrilaterals grafted in a substrate

Here, we study the elasticity of N number of the longitudinally connected quadrilaterals. The symmetry of the system implies that it is equivalent to a system consisting of N number of springs in series in a way that each spring has a Poisson's ratio of $\nu_1 = \cot^2(\omega)/2$ which is equals to the Poisson's ratio of a grafted quadrilateral (see eqn (15)). Also, the force constant of each spring in x coordinate is equals to the force constant of a grafted quadrilateral in x coordinate, $k = 6k_{\mathrm{B}} T l_{\mathrm{p}}/L^3(\sin(\omega))^2$ (see eqn (12)). The force constant of N number of the springs in series is k/N (Fig. 3). Therefore, the force–extension relation of a system with the N number of the longitudinally connected quadrilaterals in x coordinate is

$$
\left\langle f_{\omega,N}^{\mathrm{LO},X}(x) \right\rangle = -\frac{6k_{\mathrm{B}} T l_{\mathrm{p}}(x - H_N)}{NL^3 (\sin(\omega))^2} \tag{30}
$$

where the length of the system in x direction is $H_N = 2NL\cos(\omega)$. The probability density of the x component of position of the tip of the polymeric system is

$$
P_{\omega,N}^{\mathrm{LO},X}(x) = \frac{1}{N_{\omega,2}^{\mathrm{LO},X}} \exp\left(-\frac{3}{N} \frac{l_{\mathrm{p}}(x - H_N)^2}{L^3(\sin(\omega))^2} \right) \tag{31}
$$

Also, the Poisson's ratio of the system consisting of N number of springs is

$$
\nu_{\mathrm{N}} = \frac{\dfrac{\Delta y}{w}}{\dfrac{\Delta x}{H_N}} = \frac{1}{2}\cot^2(\omega) \tag{32}
$$

where Δx is the displacement of the tip of the system in the longitudinal direction and Δy is the contraction or the expansion of the system in the transverse direction.

Again, we confine the system with a stiff wall in x coordinate and calculate the average of the fluctuating force on the wall. The average of the exerted fluctuating force on the confining stiff wall by the fluctuating tip of the system is (see Appendix),

$$
\left\langle f_{\omega,N}^{\mathrm{Wall}-X}(\delta) \right\rangle = \left(\frac{12l_{\mathrm{p}}}{N\pi L^3} \right)^{\frac{1}{2}} \left(\frac{k_{\mathrm{B}} T e^{-\frac{3l_{\mathrm{p}}(\delta - H_N)^2}{NL^3 \sin(\omega)}}}{A_N} \right) \tag{33}
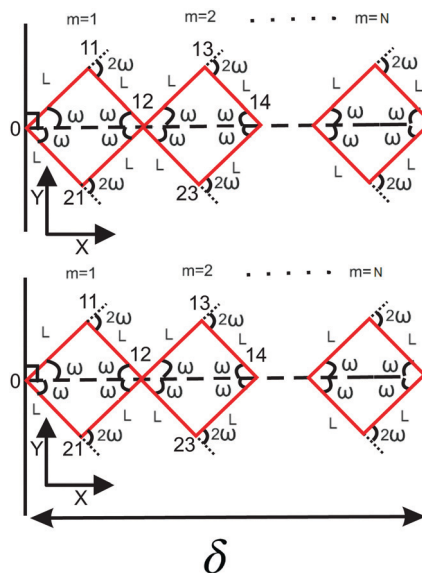$$

Fig. 3 The upper panel: The configuration of the grafted N number of the longitudinally connected quadrilaterals at zero temperature. The lower panel: The N number of the longitudinally connected quadrilaterals confined by a stiff planar wall.

where

$$
A_N = \sin(\omega) \left(\mathrm{erf}\left(\left(\frac{12Nl_{\mathrm{p}}}{L} \right)^{\frac{1}{2}} \cot(\omega) \right) - \mathrm{erf}\left(\left(\frac{3l_{\mathrm{p}}}{NL^3} \right)^{\frac{1}{2}} \frac{H_N - \delta}{\sin(\omega)} \right) \right) \tag{34}
$$

2.5 Comparison of the longitudinally connected quadrilaterals with different number of quadrilaterals having the same polymeric materials

Here, we vary the number of quadrilaterals in the system of longitudinally connected quadrilaterals while we keep the total contour length of the systems (the polymeric material of the system) the same. The force–extension relation of a system with the N number of the longitudinally connected quadrilaterals in x coordinate is (see eqn (30))

$$
\left\langle f_{\omega,N}^{\mathrm{LO},X}(x) \right\rangle = -\frac{384 N^2 k_{\mathrm{B}} T l_{\mathrm{p}}(x - H_N)}{L_{\mathrm{PM}}^3 (\sin(\omega))^2} \tag{35}
$$

where $L_{\mathrm{PM}} = 4NL$ is the total contour length of the system. The force constant associated with the force–extension relation is $K_x = \dfrac{384 N^2 k_{\mathrm{B}} T l_{\mathrm{p}}}{L_{\mathrm{PM}}^3 \sin^2(\omega)}$. The dimensionless form of the force–extension relation is

$$
\left\langle \tilde{f}_{\omega,N}^{\mathrm{LO},X}(x) \right\rangle = \frac{L_{\mathrm{PM}} \left\langle f_{\omega,N}^{\mathrm{LO},X}(x) \right\rangle}{k_{\mathrm{B}} T} = -\frac{384 N^2 l_{\mathrm{p}}(x - H_N)}{L_{\mathrm{PM}}^2 (\sin(\omega))^2} \tag{36}
$$

and the dimensionless force constant is $\tilde{K}_x = \dfrac{K_x L_{\mathrm{PM}}^2}{k_{\mathrm{B}} T} = \dfrac{384 N^2 l_{\mathrm{p}}}{L_{\mathrm{PM}} \sin^2(\omega)}$. If we keep the polymeric material of the system (L_{PM}) fixed, the force constant will depend on the squared of the

number of quadrilaterals. The higher the force constant, the stiffer the system. This fact shows that the system with higher number of quadrilateral with the same amount of polymeric material is stiffer as it can be seen from eqn (36).

It is interesting that the Poisson's ratio is independent of amount of the polymeric material used in the system (the total contour length) and only depends on the angle ω (see eqn (32))

$$\nu_N = \frac{1}{2}\cot^2(\omega) \qquad (37)$$

The average of the exerted fluctuating force on the confining stiff wall by the fluctuating tip of the system with the fixed total polymeric length, L_{PM} is (see eqn (33))

$$\left\langle f_{\omega,N}^{\text{Wall}-X}(\delta) \right\rangle = \left(\frac{768N^2 l_p}{\pi L_{PM}^3}\right)^{\frac{1}{2}} \left(\frac{k_B T e^{-\frac{192N^2 l_p(\delta - H_N)^2}{L_{PM}^3 \sin(\omega)}}}{A_N}\right) \qquad (38)$$

where

$$A_N = \sin(\omega)\left(\text{erf}\left(\left(\frac{48N^2 l_p}{L_{PM}}\right)^{\frac{1}{2}}\cot(\omega)\right)\right.$$
$$\left. -\text{erf}\left(\left(\frac{192N^2 l_p}{L_{PM}^3}\right)^{\frac{1}{2}}\frac{H_N - \delta}{\sin(\omega)}\right)\right) \qquad (39)$$

The dimensionless form of the average of the force on the wall is

$$\left\langle \tilde{f}_{\omega,N}^{\text{Wall}-X}(\delta) \right\rangle = \frac{L_{PM}\left\langle f_{\omega,N}^{\text{Wall}-X}(\delta)\right\rangle}{k_B T}$$
$$= \left(\frac{768N^2 l_p}{\pi L_{PM}}\right)^{\frac{1}{2}}\left(\frac{e^{-\frac{192N^2 l_p(\delta - H_N)^2}{L_{PM}^3 \sin(\omega)}}}{A_N}\right) \qquad (40)$$

Fig. 4 shows the average of the dimensionless force exerted to the wall by the system of the longitudinally connected quadrilaterals. We fix the polymeric material of the system and vary the number of the quadrilaterals for different curves. We look at the force–extension curves in two different regimes. In the first regime, $\delta < H_N$, the system is compressed by the wall therefore the mixture of the entropic forces and enthalpic forces play role in the elasticity of the system. In this regime, the force constant of the system increases as the number of quadrilaterals increases. In the second regime, $\delta > H_N$, the system is not compressed therefore the entropic forces play major role in the elasticity of the system. In this regime the system should be bent by the thermal fluctuations to hit the wall therefore the dimensionless force exerted to the wall decreases as the number of the quadrilaterals increases. In Fig. 5, we show the force–extension relation of the wall while we vary the value of the persistence length for the different curves. The force constant of the system increases in the regime, $\delta < H_N$, while the persistence length increases. We expected this fact since the system should be stiffer for higher values of the persistence length. In Fig. 6, we show the
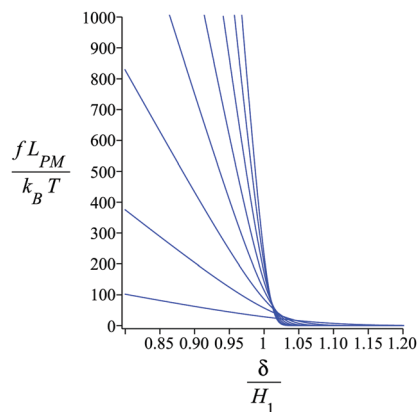

Fig. 4 The force–extension relation of the wall (the solutions of eqn (38)) is shown for different number of the quadrilaterals (N = 1, 2, 3, 4, 5, 6, 7, 8) while the polymeric material of the system is kept fixed. The higher the absolute value of the force constant (slope of the curve) in the range $\delta < H_N$ the higher the number of the quadrilaterals. The fixed parameters are: $k_B T$ = 4.114 pN nm, l_p = 50 nm, L_{PM} = 30 nm, $\omega = \frac{\pi}{4}$ and $L = \frac{L_{PM}}{4N}$.
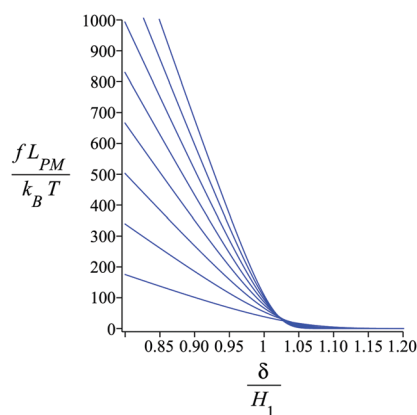

Fig. 5 The force–extension relation of the wall (the solutions of eqn (38)) is shown for different persistence length (l_p = 10 nm, 20 nm, 30 nm, 40 nm, 50 nm, 60 nm, 70 nm, 80 nm) while the polymeric material of the system is kept fixed. The higher the absolute value of the force constant (slope of the curve) in the range $\delta < H_N$ the higher the persistence length. The fixed parameters are: $k_B T$ = 4.114 pN nm, N = 3, L_{PM} = 30 nm, $\omega = \frac{\pi}{4}$ and $L = \frac{L_{PM}}{4N}$.

force–extension of the wall for different values of the angle, ω. The stiffness of the system increases as the value of the angle, ω decreases (Fig. 6).

3 Discussion and conclusion

Here, we employed the worm-like chain model to describe the elastic behavior of a system made of longitudinally connected quadrilaterals. To obtain analytic expressions for the probability densities associated with the thermal fluctuation of the tip and the corners of the system, we used a positional–orientational propagator of a semiflexible filament in the weakly bending regime, which was introduced in ref. 6, 87 and 88. We used the
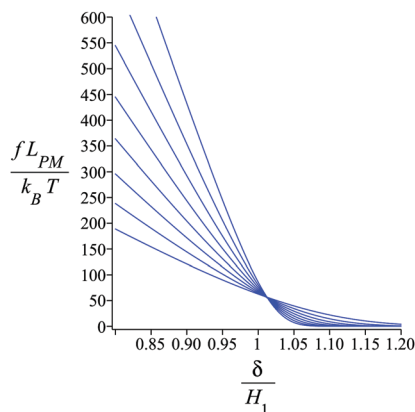
Fig. 6 The force–extension relation of the wall (the solutions of eqn (38)) is shown for different angles, $\left(\omega = \frac{\pi}{4} + \frac{\pi i}{6 \times 7}\right)$ where i = 0, 1, 2, 3, 4, 5, 6, 7. The higher the absolute value of the force constant (slope of the curve) in the range $\delta < H_N$ the lower the value of ω. The fixed parameters are: $k_B T$ = 4.114 pN nm, N = 3, l_p = 50 nm, L_{PM} = 30 nm, N = 3 and $L = \frac{L_{PM}}{4N}$.

probability densities to calculate the force–extension relation of the tip of the system for arbitrary number of the quadrilaterals in the fixed extension ensemble. We offered a closed analytic expression which is valid in the linear regime (since we used the weakly bending approximation). The force constant associated with the force–extension relation is proportional to the bending stiffness, κ and the squared of the number of the quadrilaterals, N^2 and it is reversely proportional to the cubed of the total contour length (the amount of the polymeric material), L_{PM}^3 and $\sin^2(\omega)$. Also, we obtained an analytic expression for the Poisson's ratio of the system. It only depends on the angle, ω. The Poisson's ratio does not depend on the amount of polymeric material or the bending stiffness; therefore, it is a geometrical quantity of our system. In the last step, we confined the system with a planar stiff wall and calculated the average of the force exerted to the wall. The analytic expression for the average of the force depends on the persistence length, l_p, total contour length, L_{PM}, thermal energy, $k_B T$, the number of the quadrilaterals, N, the angle, ω and the distance of the wall from the grafting point of the system, δ. All of the relations obtained in this article are closed analytic expressions therefore it is easy to theoretically track the behavior of the system in the parameter space of the linear force regime.

The theoretical model presented here can be applied to experimental and molecular modeling data available from research into DNA minicircles. Michele Caraglio et al. studied the DNA minicircles confined in a two dimensional space by a course grained model called the oxDNA.[89] The oxDNA has two versions. The first version uses the symmetric grooves and is called the oxDNA1. The second version is implemented with asymmetric grooves. They reported rounded square shape for the case of the oxDNA1 and a circular shape for the case of oxDNA2 when the DNA minicircle is confined in a two dimensional space.[89] Our calculations can be used to describe the two dimensional bending elasticity of the square shape of the DNA

appeared in the model of oxDNA1. The bending modes of the DNA minicircles were studied by Davide Demurtas et al.[90] A molecular dynamics study of minicircles was done by Marco Pasi et al.[91] A theoretical study of the effect of bending anisotropy in minicircles is available in ref. 92. The circular shape of the DNA minicircles can be approximated with a square and then our model can be applied to describe the bending elasticity of them. The square shape structure made of the DNA is reported in ref. 93. Sungwook Woo et al. experimentally studied the self-assembly of two-dimensional DNA origami.[94] They report a two dimensional square shape of DNA that can be arrange in one dimensional and two dimensional lattice. The elasticity of the one dimensional lattice made of squares of the DNA can be studied by our model (see Fig. 5 in ref. 94). The model presented in our article can be easily modified for describing the bending elasticity of semiflexible polymeric materials of more complex topologies which we suggest for future work.

Conflicts of interest

There are no conflicts to declare.

Appendix

A.1. The force–extension relation in the fixed-extension ensemble

Here, we consider a system made of a semiflexible polymer which is described by a Hamiltonian, H. We can look at the probability density function of the position of a fluctuating tip of a polymeric system in x coordinate as a partition function,[88]

$$P^X(x) = \int Dr(s) \exp\left(-\frac{H}{k_B T}\right) \delta(r_x(L) - x) \tag{41}$$

where $r(s) = (r_x(s), r_y(s), r_z(t))$ is the position vector associate with the arc length s and $r_x(L)$ is the position of the tip of the system in x coordinate. The partition function is in the fixed position ensemble because of the term, $\delta(r_x(L) - x)$ which fixes the x component of the position of the tip in the value, x. The partition function gives the following term for the free energy associated with the tip,

$$F^X(x) = -k_B T \ln(P^X(x)) \tag{42}$$

The free energy defines the average of the x component of the force exerted to the tip in the fixed extension ensemble,

$$\langle f^X(x) \rangle = -\frac{dF^X(x)}{dx} = k_B T \frac{d}{dx} \ln(P^X(x)) \tag{43}$$

This is the force–extension relation the fixed extension ensemble. The experimental setup for measuring the relation should be build in a way that the position of the tip in x coordinate is fixed while the other components of the position are free. In the experimental setup the force exerted in x coordinate would thermally fluctuate. By the similar reasoning we can obtain a force–extension relation in y coordinate,

$$\langle f^Y(y) \rangle = k_B T \frac{d}{dy} \ln(P^Y(y)) \tag{44}$$

where $P^y(y)$ is the probability density function of the position of a fluctuating tip of a polymeric system in y coordinate. In the next subsections, we will use eqn (43) and (44) to calculate the force–extension relation associated with the connected quadrilaterals.

A.2. The Poisson's ratio

Here, we calculate the Poisson's ratio of a system. To do so, we consider the case of one grafted quadrilateral (see Fig. 2) and calculate the y component of displacement of the lateral point of the quadrilateral labeled by 11 in due to the displacement of the tip labeled by 12 in x coordinate. The probability density of the x component of the position if the tip of the quadrilateral (labeled by 12) is shown by $P^X_{\omega,1}(x_{12})$. The force–extension relation associated with the probability density is

$$\left\langle f^X_{\omega,1}(x_{12})\right\rangle = k_B T \frac{\mathrm{d}}{\mathrm{d}x_{12}}\ln\left(P^X_{\omega,1}(x_{12})\right) \tag{45}$$

where $\langle f^X_{12}(x_{12})\rangle$ is the average of the fluctuating force in x coordinate that keeps the x component of extension of the tip labeled by 12 in the fixed value of x_{12} while the other points of the quadrilateral are free.

The probability density to find the x component of the position of the corner labeled by 12 at x_{12} and the y component of the position of the corner labeled by 11 at y_{11} is shown by $P^{PR}_{\omega,1}(x_{12},y_{11})$. The force–extension relation associated with the probability density is given be the following equation,

$$\left\langle f^{PR}_{\omega,1}(x_{12},y_{11})\right\rangle = k_B T \frac{\mathrm{d}}{\mathrm{d}x_{12}}\ln\left(P^{PR}_{\omega,1}(x_{12},y_{11})\right) \tag{46}$$

where $\langle f^X_{12}(x_{12},y_{11})\rangle$ is the average of the fluctuating force in x coordinate that keeps the x component of position of the tip labeled by 12 in the fixed value of x_{12} and the y component of position of the point labeled by 11 in the fixed value of y_{11} while the other points of the quadrilateral are free. The condition $\langle f^{PR}_{\omega,1}(x_{12},y_{11})\rangle = \langle f^X_{\omega,1}(x_{12})\rangle$ gives the relation between y_{11} and the fixed value of x_{12}. Inserting eqn (45) and (46) in the condition, we find the relation between the lateral contraction or the lateral expansion of the system due to the longitudinal displacement of the end point of the system

$$\frac{\mathrm{d}}{\mathrm{d}x_{12}}\ln\left(P^X_{\omega,1}(x_{12})\right) = \frac{\mathrm{d}}{\mathrm{d}x_{12}}\ln\left(P^{PR}_{\omega,1}(x_{12},y_{11})\right) \tag{47}$$

We define the Poisson's ratio of the quadrilateral as follows,

$$\nu_1 = -\frac{\dfrac{y_{11}-L\sin(\omega)}{2L\sin(\omega)}}{\dfrac{x_{12}-2L\cos(\omega)}{2L\cos(\omega)}} \tag{48}$$

A.3. The force exerted to a stiff confining wall by a fluctuating tip

Here, we take the grafted quadrilateral as an example of the polymeric system and confine the system by a stiff and impenetrable wall in x coordinate. The distance of the wall from the grafting point of the quadrilateral is fixed, δ while the fluctuating tip of the quadrilateral exerts a fluctuating force on the wall. We are interested in calculating the average of the
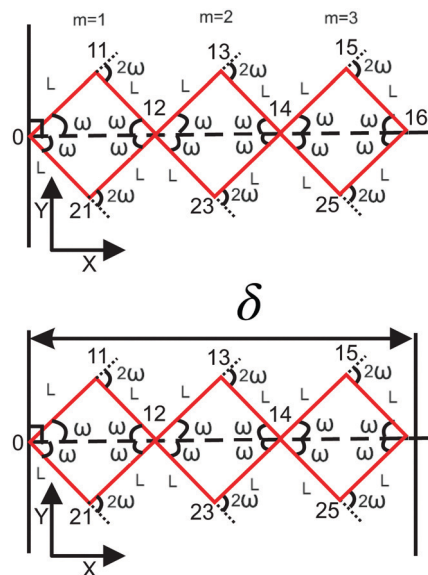

Fig. 7 The upper panel: The configuration of the grafted three longitudinally connected quadrilaterals at zero temperature. The lower panel: The three longitudinally connected quadrilaterals confined by a stiff planar wall.

force (see Fig. 1, 2 and 7). To do so, we use the method introduced in ref. 6 and 95. The origin of the force comes from the reduction of the number of the configuration of the system due to the presence of the wall. The number of the configuration of the system is given by the following equation[6,95]

$$Z(\delta) = \int_0^\delta P^X_{\omega,1}(x_{12})\mathrm{d}x_{12} \tag{49}$$

where $P^X_{\omega,1}(x_{12})$ is the probability density to find the x component of the position of the tip of the quadrilateral at the value, x_{12}. The derivative of the logarithm of the number of the configuration of the system with respect to δ is the average of the fluctuating force

$$\left\langle f^{\mathrm{Wall}-X}_{\omega,1}(\delta)\right\rangle = k_B T \frac{\mathrm{d}}{\mathrm{d}\delta}\ln(Z(\delta)) \tag{50}$$

In this method, we ignore the steric effect of the wall and the other corners of the system.

A.4. Three longitudinally connected quadrilaterals grafted in a substrate

The probability density to find the end point of the grafted three longitudinally connected quadrilateral in position (x_{16},y_{16}) and orientation, θ_{16} is

$$\begin{aligned}
P^{LO}_{\omega,3}(x_{16},y_{16},\theta_{16}) = \iint \cdots \iint & G_L(x_{15},y_{15},\theta_{15}|x,y,\theta+2\omega) \\
& \times G_L(x_{16},y_{16},\theta_{16}|x_{15},y_{15},\theta_{15}-2\omega) \\
& \times P^{LO}_{\omega,2}(x,y,\theta)G_L(x_{25},y_{25},\theta_{25}|x,y,\theta) \\
& \times G_L(x_{16},y_{16},\theta_{16}+2\omega|x_{25},y_{25},\theta_{25}+2\omega) \\
& \times \mathrm{d}x_{15}\mathrm{d}y_{15}\mathrm{d}\theta_{15}\mathrm{d}x_{25}\mathrm{d}y_{25}\mathrm{d}\theta_{25}\mathrm{d}x\mathrm{d}y\mathrm{d}\theta
\end{aligned}$$

$$\tag{51}$$

We obtain the probability density to find the position of the end point of the structure in x coordinate at value x according to below,

$$
\begin{aligned}
P_{\omega,3}^{\mathrm{LO},X}(x) &= \iint P_{\omega,3}^{\mathrm{LO}}(x,y,\theta)\mathrm{d}y\mathrm{d}\theta \\
&= \frac{1}{N_{\omega,3}^{\mathrm{LO},X}}\exp\left(-\frac{l_{\mathrm{p}}(x^2+6L\cos(\omega))^2}{L^3(\sin(\omega))^2}\right)
\end{aligned}
\tag{52}
$$

Similarly, the probability density to find the position of the end point of the structure in y coordinate at value y is of the following form,

$$
\begin{aligned}
P_{\omega,3}^{\mathrm{LO},Y}(y) &= \iint P_{\omega,3}^{\mathrm{LO}}(x,y,\theta)\mathrm{d}x\mathrm{d}\theta \\
&= \frac{1}{N}\exp\left(-\frac{1}{39}\frac{l_{\mathrm{p}}y^2}{(\cos(\omega))^2 L^3}\right)
\end{aligned}
\tag{53}
$$

The force–extension relation in x coordinate result from the probability density function according to below (see Appendix),

$$
\left\langle f_{\omega,3}^{\mathrm{LO},X}(x)\right\rangle = k_{\mathrm{B}}T\frac{\partial}{\partial x}\ln\left(P_{\omega,3}^{\mathrm{LO},X}(x)\right) = -\frac{2k_{\mathrm{B}}Tl_{\mathrm{p}}(x-H_3)}{L^3(\sin(\omega))^2}
\tag{54}
$$

where $H_3 = 6L\cos(\omega)$. Similarly, we obtain the force–extension relation in y coordinate (see Appendix),

$$
\left\langle f_{\omega,3}^{\mathrm{LO},Y}(y)\right\rangle = k_{\mathrm{B}}T\frac{\partial}{\partial y}\ln\left(P_{\omega,3}^{\mathrm{LO},Y}(y)\right) = -\frac{2}{39}\frac{k_{\mathrm{B}}Tl_{\mathrm{p}}y}{(\cos(\omega))^2 L^3}
\tag{55}
$$

To calculate the Poisson's ratio, we have to calculate the following quantity (see Appendix),

$$
\begin{aligned}
P_{\omega,3}^{\mathrm{PR}}(x_{16},y_{15}) = \iint\cdots\iint & G_{\mathrm{L}}(x_{15},y_{15},\theta_{15}|x,y,\theta+2\omega) \\
& \times G_{\mathrm{L}}(x_{16},y_{16},\theta_{16}|x_{15},y_{15},\theta_{15}-2\omega) \\
& \times P_{\omega,2}^{\mathrm{LO}}(x,y,\theta)G_{\mathrm{L}}(x_{25},y_{25},\theta_{25}|x,y,\theta) \\
& \times G_{\mathrm{L}}(x_{16},y_{16},\theta_{16}+2\omega|x_{25},y_{25},\theta_{25}+2\omega) \\
& \times \mathrm{d}x_{15}\mathrm{d}\theta_{15}\mathrm{d}x_{25}\mathrm{d}y_{25}\mathrm{d}\theta_{25}\mathrm{d}x\mathrm{d}y\mathrm{d}\theta
\end{aligned}
\tag{56}
$$

which is the probability density to find the x component of the position of the corner labeled by 16 at the value of x_{16} and the y component of the position of the point labeled by 15 at the value of y_{15}. The relation between the displacement in lateral direction and the displacement in longitudinal direction is given by the following equation,

$$
k_{\mathrm{B}}T\frac{\partial}{\partial x}\ln\left(P_{\omega,3}^{\mathrm{PR}}(x,y_{15})\right) = k_{\mathrm{B}}T\frac{\partial}{\partial x}\ln\left(P_{\omega,3}^{X}(x)\right)
\tag{57}
$$

which is of the following form

$$
\frac{y_{15}-L\sin(\omega)}{x-6L\cos(\omega)} = -\frac{1}{6}\cot(\omega)
\tag{58}
$$

where $y_{115} - L\sin(\omega)$ is the displacement of the corner of the quadrilateral labeled by 15 in y coordinate due to the

displacement of the corner labeled by 16 in x coordinate, $x - 6L\cos(\omega)$. Therefore the Poisson's ratio is

$$
\nu_3 = -\frac{\dfrac{y_{15}-L\sin(\omega)}{W}}{\dfrac{x-6L\cos(\omega)}{H_3}} = \frac{1}{2}\cot^2(\omega)
\tag{59}
$$

As with the previous section, if we confine the system by a stiff wall in x coordinate the wall will experience a fluctuating force. The average of the fluctuating force on the confining stiff wall is (see Appendix)

$$
\left\langle f_{\omega,3}^{\mathrm{Wall}-X}(\delta)\right\rangle = \left(\frac{4l_{\mathrm{p}}}{\pi L^3}\right)^{\frac{1}{2}}\left(\frac{k_{\mathrm{B}}Te^{-\frac{l_{\mathrm{p}}(\delta-H_3)^2}{L^3\sin(\omega)}}}{A_3}\right)
\tag{60}
$$

where

$$
A_3 = \sin(\omega)\left(\mathrm{erf}\left(\left(\frac{36l_{\mathrm{p}}}{L}\right)^{\frac{1}{2}}\cot(\omega)\right) - \mathrm{erf}\left(\left(\frac{l_{\mathrm{p}}}{L^3}\right)^{\frac{1}{2}}\frac{H_3-\delta}{\sin(\omega)}\right)\right)
\tag{61}
$$

Acknowledgements

Notes and references

1 D. A. Fletcher and R. D. Mullins, *Nature*, 2010, **463**, 485–492.
2 A. Chaigne, C. Campillo, R. Voituriez, N. S. Gov, C. Sykes, M.-H. Verlhac and M.-E. Terret, *Nat. Commun.*, 2016, 7, 1–14.
3 R. Zhang, N. Kumar, J. L. Ross, M. L. Gardel and J. J. De Pablo, *Proc. Natl. Acad. Sci. U. S. A.*, 2018, **115**, E124–E133.
4 P. A. Janmey, S. Hvidt, J. Käs, D. Lerche, A. Maggs, E. Sackmann, M. Schliwa and T. P. Stossel, *J. Biol. Chem.*, 1994, **269**, 32503–32513.
5 L. Blanchoin, R. Boujemaa-Paterski, C. Sykes and J. Plastino, *Physiol. Rev.*, 2014, **94**, 235–263.
6 M. Razbin, M. Falcke, P. Benetatos and A. Zippelius, *Phys. Biol.*, 2015, **12**, 046007.
7 D. E. Dupuis, W. H. Guilford, J. Wu and D. Warshaw, *J. Muscle Res. Cell Motil.*, 1997, **18**, 17–30.
8 F. Rückerl, M. Lenz, T. Betz, J. Manzi, J.-L. Martiel, M. Safouane, R. Paterski-Boujemaa, L. Blanchoin and C. Sykes, *Biophys. J.*, 2017, **113**, 1072–1079.
9 S. Walcott and S. X. Sun, *Proc. Natl. Acad. Sci. U. S. A.*, 2010, **107**, 7757–7762.
10 K. Kasza, C. Broedersz, G. Koenderink, Y. Lin, W. Messner, E. Millman, F. Nakamura, T. Stossel, F. MacKintosh and D. Weitz, *Biophys. J.*, 2010, **99**, 1091–1100.
11 M. Gardel, J. H. Shin, F. MacKintosh, L. Mahadevan, P. Matsudaira and D. Weitz, *Science*, 2004, **304**, 1301–1305.

12 M. Guo, A. J. Ehrlicher, S. Mahammad, H. Fabich, M. H. Jensen, J. R. Moore, J. J. Fredberg, R. D. Goldman and D. A. Weitz, *Biophys. J.*, 2013, **105**, 1562–1568.

13 N. Wang and D. Stamenovic, *J. Muscle Res. Cell Motil.*, 2002, **23**, 535–540.

14 P. Pawelzyk, N. Mücke, H. Herrmann and N. Willenbacher, *PLoS One*, 2014, **9**, e93194.

15 W. H. Goldmann, *Cell Biol. Int.*, 2018, **42**, 132–138.

16 L. Kreplak and D. Fudge, *BioEssays*, 2007, **29**, 26–35.

17 D. S. Fudge, K. H. Gardner, V. T. Forsyth, C. Riekel and J. M. Gosline, *Biophys. J.*, 2003, **85**, 2015–2027.

18 S. Köster, D. A. Weitz, R. D. Goldman, U. Aebi and H. Herrmann, *Curr. Opin. Cell Biol.*, 2015, **32**, 82–91.

19 G. J. Brouhard and L. M. Rice, *Nat. Rev. Mol. Cell Biol.*, 2018, **19**, 451–463.

20 S. Forth and T. M. Kapoor, *J. Cell Biol.*, 2017, **216**, 1525–1531.

21 T. Li, *J. Biomech.*, 2008, **41**, 1722–1729.

22 D. K. Fygenson, J. F. Marko and A. Libchaber, *Phys. Rev. Lett.*, 1997, **79**, 4497.

23 T. Hawkins, M. Mirigian, M. S. Yasar and J. L. Ross, *J. Biomech.*, 2010, **43**, 23–30.

24 D. Havelka, M. A. Deriu, M. Cifra and O. Kučera, *Sci. Rep.*, 2017, **7**, 1–11.

25 J. Howard and A. A. Hyman, *Nature*, 2003, **422**, 753–758.

26 T. R. Strick, J.-F. Allemand, D. Bensimon, A. Bensimon and V. Croquette, *Science*, 1996, **271**, 1835–1837.

27 M. Rief, H. Clausen-Schaumann and H. E. Gaub, *Nat. Struct. Biol.*, 1999, **6**, 346–349.

28 C. Bustamante, Z. Bryant and S. B. Smith, *Nature*, 2003, **421**, 423–427.

29 C. Bustamante, S. B. Smith, J. Liphardt and D. Smith, *Curr. Opin. Struct. Biol.*, 2000, **10**, 279–285.

30 J. F. Marko and E. D. Siggia, *Macromolecules*, 1995, **28**, 8759–8770.

31 A. Ahsan, J. Rudnick and R. Bruinsma, *Biophys. J.*, 1998, **74**, 132–137.

32 C. Bouchiat and M. Mezard, *Phys. Rev. Lett.*, 1998, **80**, 1556.

33 J. F. Marko and E. D. Siggia, *Macromolecules*, 1994, **27**, 981–988.

34 M. D. Wang, H. Yin, R. Landick, J. Gelles and S. M. Block, *Biophys. J.*, 1997, **72**, 1335.

35 M. Heidari, H. Schiessel and A. Mashaghi, *ACS Cent. Sci.*, 2020, **6**(6), 839–847, DOI: 10.1021/acscentsci.0c00308.

36 B. Scalvini, V. Sheikhhassani, J. Woodard, J. Aupič, R. T. Dame, R. Jerala and A. Mashaghi, *Trends Chem.*, 2020, **2**(7), 609–622, DOI: https://doi.org/10.1016/j.trechm.2020.04.009.

37 C. A. Mirkin, R. L. Letsinger, R. C. Mucic and J. J. Storhoff, *Nature*, 1996, **382**, 607–609.

38 C. M. Niemeyer, W. Bürger and J. Peplies, *Angew. Chem., Int. Ed.*, 1998, **37**, 2265–2268.

39 K. Keren, M. Krueger, R. Gilad, G. Ben-Yoseph, U. Sivan and E. Braun, *Science*, 2002, **297**, 72–75.

40 W. E. Ford, O. Harnack, A. Yasuda and J. M. Wessels, *Adv. Mater.*, 2001, **13**, 1793–1797.

41 A. P. Alivisatos, K. P. Johnsson, X. Peng, T. E. Wilson, C. J. Loweth, M. P. Bruchez and P. G. Schultz, *Nature*, 1996, **382**, 609–611.

42 D. Nykypanchuk, M. M. Maye, D. Van Der Lelie and O. Gang, *Nature*, 2008, **451**, 549–552.

43 Y. Zhang, F. Lu, K. G. Yager, D. Van Der Lelie and O. Gang, *Nat. Nanotechnol.*, 2013, **8**, 865–872.

44 A. R. Chandrasekaran and O. Levchenko, *Chem. Mater.*, 2016, **28**, 5569–5581.

45 C. E. Castro, F. Kilchherr, D.-N. Kim, E. L. Shiao, T. Wauer, P. Wortmann, M. Bathe and H. Dietz, *Nat. Methods*, 2011, **8**, 221.

46 P. W. Rothemund, *Nature*, 2006, **440**, 297–302.

47 L. Qian, Y. Wang, Z. Zhang, J. Zhao, D. Pan, Y. Zhang, Q. Liu, C. Fan, J. Hu and L. He, *Chin. Sci. Bull.*, 2006, **51**, 2973–2976.

48 S. M. Douglas, J. J. Chou and W. M. Shih, *Proc. Natl. Acad. Sci. U. S. A.*, 2007, **104**, 6644–6648.

49 E. S. Andersen, M. Dong, M. M. Nielsen, K. Jahn, A. Lind-Thomsen, W. Mamdouh, K. V. Gothelf, F. Besenbacher and J. Kjems, *ACS Nano*, 2008, **2**, 1213–1218.

50 Y. Ke, J. Sharma, M. Liu, K. Jahn, Y. Liu and H. Yan, *Nano Lett.*, 2009, **9**, 2445–2447.

51 E. S. Andersen, M. Dong, M. M. Nielsen, K. Jahn, R. Subramani, W. Mamdouh, M. M. Golas, B. Sander, H. Stark and C. L. Oliveira, *et al.*, *Nature*, 2009, **459**, 73–76.

52 E. Pound, J. R. Ashton, H. A. Becerril and A. T. Woolley, *Nano Lett.*, 2009, **9**, 4302–4305.

53 D. Han, S. Pal, Y. Liu and H. Yan, *Nat. Nanotechnol.*, 2010, **5**, 712–717.

54 W. Liu, H. Zhong, R. Wang and N. C. Seeman, *Angew. Chem., Int. Ed.*, 2011, **50**, 264–267.

55 B. Saccà, R. Meyer, M. Erkelenz, K. Kiko, A. Arndt, H. Schroeder, K. S. Rabe and C. M. Niemeyer, *Angew. Chem.*, 2010, **122**, 9568–9573.

56 N. C. Seeman, *Structural DNA nanotechnology*, Cambridge University Press, 2015.

57 K. Lund, A. J. Manzo, N. Dabby, N. Michelotti, A. Johnson-Buck, J. Nangreave, S. Taylor, R. Pei, M. N. Stojanovic and N. G. Walter, *et al.*, *Nature*, 2010, **465**, 206–210.

58 E. Winfree, F. Liu, L. A. Wenzler and N. C. Seeman, *Nature*, 1998, **394**, 539–544.

59 S. M. Douglas, H. Dietz, T. Liedl, B. Högberg, F. Graf and W. M. Shih, *Nature*, 2009, **459**, 414–418.

60 H. Dietz, S. M. Douglas and W. M. Shih, *Science*, 2009, **325**, 725–730.

61 D. Han, S. Pal, J. Nangreave, Z. Deng, Y. Liu and H. Yan, *Science*, 2011, **332**, 342–346.

62 K. E. Dunn, F. Dannenberg, T. E. Ouldridge, M. Kwiatkowska, A. J. Turberfield and J. Bath, *Nature*, 2015, **525**, 82–86.

63 F. Zhang, S. Jiang, S. Wu, Y. Li, C. Mao, Y. Liu and H. Yan, *Nat. Nanotechnol.*, 2015, **10**, 779.

64 E. Benson, A. Mohammed, J. Gardell, S. Masich, E. Czeizler, P. Orponen and B. Högberg, *Nature*, 2015, **523**, 441–444.

65 R. Veneziano, S. Ratanalert, K. Zhang, F. Zhang, H. Yan, W. Chiu and M. Bathe, *Science*, 2016, **352**, 1534.

66 J. Song, Z. Li, P. Wang, T. Meyer, C. Mao and Y. Ke, *Science*, 2017, **357**(6349), DOI: 10.1126/science.aan3377.

67 E. Kopperger, J. List, S. Madhira, F. Rothfischer, D. C. Lamb and F. C. Simmel, *Science*, 2018, **359**, 296–301.

68 H. Jun, F. Zhang, T. Shepherd, S. Ratanalert, X. Qi, H. Yan and M. Bathe, *Sci. Adv.*, 2019, **5**, eaav0655.

69 N. C. Seeman, *DNA Nanotechnology*, Springer, 2018, pp. 1–9.

70 H.-P. Hsu, W. Paul and K. Binder, *EPL*, 2010, **92**, 28003.

71 J. Z. Chen, *Prog. Polym. Sci.*, 2016, **54**, 3–46.

72 M. Razbin, P. Benetatos and A. Zippelius, *Phys. Rev. E*, 2016, **93**, 052408.

73 R. G. Winkler, *J. Chem. Phys.*, 2003, **118**, 2919–2928.

74 L. Livadaru, R. Netz and H. Kreuzer, *Macromolecules*, 2003, **36**, 3732–3744.

75 C. Heussinger, M. Bathe and E. Frey, *Phys. Rev. Lett.*, 2007, **99**, 048101.

76 J. Wilhelm and E. Frey, *Phys. Rev. Lett.*, 1996, **77**, 2581.

77 R. Vlijm, A. Mashaghi, S. Bernard, M. Modesti and C. Dekker, *Nanoscale*, 2015, **7**, 3205–3216.

78 S. Bezrukavnikov, A. Mashaghi, R. J. van Wijk, C. Gu, L. J. Yang, Y. Q. Gao and S. J. Tans, *Soft Matter*, 2014, **10**, 7269–7277.

79 K. C. Neuman and A. Nagy, *Nat. Methods*, 2008, **5**, 491–505.

80 T. Strick, M. Dessinges, G. Charvin, N. Dekker, J. Allemand, D. Bensimon and V. Croquette, *Rep. Prog. Phys.*, 2002, **66**, 1.

81 J. R. Moffitt, Y. R. Chemla, S. B. Smith and C. Bustamante, *Annu. Rev. Biochem.*, 2008, **77**(1), 205–228, DOI: 10.1146/annurev.biochem.77.043007.090225.

82 S. B. Smith, L. Finzi and C. Bustamante, *Science*, 1992, **258**, 1122–1126.

83 K. Kim and O. A. Saleh, *Nucleic Acids Res.*, 2009, **37**, e136.

84 M. Rief, F. Oesterhelt, B. Heymann and H. E. Gaub, *Science*, 1997, **275**, 1295–1297.

85 T. T. Perkins, D. Smith and S. Chu, *et al.*, *Science*, 1994, **264**, 822–826.

86 S. Dutta and P. Benetatos, *Soft Matter*, 2018, **14**, 6857–6866.

87 P. Benetatos and E. Frey, *Phys. Rev. E: Stat., Nonlinear, Soft Matter Phys.*, 2003, **67**, 051108.

88 M. Razbin, *J. Stat. Phys.*, 2018, **170**, 642–651.

89 M. Caraglio, E. Skoruppa and E. Carlon, *J. Chem. Phys.*, 2019, **150**, 135101.

90 D. Demurtas, A. Amzallag, E. J. Rawdon, J. H. Maddocks, J. Dubochet and A. Stasiak, *Nucleic Acids Res.*, 2009, **37**, 2882–2893.

91 M. Pasi, K. Zakrzewska, J. H. Maddocks and R. Lavery, *Nucleic Acids Res.*, 2017, **45**, 4269–4277.

92 D. Norouzi, F. Mohammad-Rafiee and R. Golestanian, *Phys. Rev. Lett.*, 2008, **101**, 168103.

93 D. Han, S. Jiang, A. Samanta, Y. Liu and H. Yan, *Angew. Chem.*, 2013, **125**, 9201–9204.

94 S. Woo and P. W. Rothemund, *Nat. Commun.*, 2014, **5**, 1–11.

95 A. Gholami, J. Wilhelm and E. Frey, *Phys. Rev. E: Stat., Nonlinear, Soft Matter Phys.*, 2006, **74**, 041803.